

pubs.acs.org/journal/ascecg Research Article

Methane Hydrate Growth Promoted by Microporous Zeolitic Imidazolate Frameworks ZIF-8 and ZIF-67 for Enhanced Methane Storage

Shurraya Denning, Ahmad A. A. Majid, Jolie M. Lucero, James M. Crawford, Moises A. Carreon,* and Carolyn A. Koh*



Cite This: ACS Sustainable Chem. Eng. 2021, 9, 9001-9010



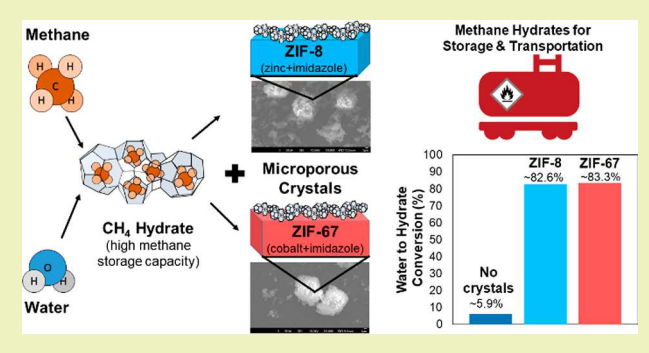
ACCESS

Metrics & More

Article Recommendations

Supporting Information

ABSTRACT: The demand for natural gas globally is rising due to the need for energy caused by population and economic growth. This demand calls for more effective approaches to store and transport natural gas, which consists primarily of methane. Gas hydrates, icelike materials that encapsulate gas molecules, possess the potential for high energy density. The feasibility of this methane storage method relies upon the efficiency of hydrate formation, which must be improved before it can be developed commercially. In this study, two microporous zeolitic imidazolate frameworks, ZIF-8 (zinc based) and ZIF-67 (cobalt based), were evaluated as methane hydrate formation promoters. ZIF-8 and ZIF-67 increased the water-to-hydrate conversion in a water-and-methane system from 4.5% to 85.6% and



87.7%, respectively, thus remarkably improving the gas storage by a factor of 14.4 and 14.7, respectively. Isothermal tests revealed that ZIF-8 and ZIF-67 reduced the methane hydrate nucleation induction time by 51.6% and 92.2%, respectively. Both ZIFs maintained their structural integrity and exhibited consistent recyclability, which indicates that the materials would have a long lifecycle as promoters. These results show that ZIF-8 and ZIF-67 are effective gas hydrate growth promoters, and application of these ZIFs makes methane storage in gas hydrates industrially appealing.

KEYWORDS: zeolitic imidazolate frameworks, methane, gas hydrates, hydrate growth promoter, gas storage

■ INTRODUCTION

The demand for energy resources continuously grows as the global economy progressively develops and as population rises. A current, efficient way to meet this demand is using natural gas, which consists primarily of methane and is abundant in areas such as shale, coal beds, and deep sea floor sediments.^{2,3} The combustion of methane is relatively clean, especially when compared to most other fossil fuels or coal, making it a highly desirable alternative energy source. 4,5 Therefore, improved methods of storing and transporting natural gas are essential to maximizing the use of this energy source. The challenge in storing and transporting natural gas stems from its low density.⁶ The current methods of increasing the storage density come with disadvantages. Storage in the form of compressed natural gas poses safety issues due to the high pressure needed and explosiveness of methane. Another method of storage being pursued involves adsorption of gas to various materials, yet most storage materials are underdeveloped and in the research phase.⁸⁻¹⁰ Transportation of natural gas often requires energy intensive processes like liquefying (which requires temperatures of 111.2K). This makes transportation inefficient, especially when transporting

from remote locations where the cost of setting up a pipeline is une conomical. $\!\!\!\!\!^{7}$

A novel, promising method for methane storage and transportation is the use of gas hydrates.^{7,11} Gas hydrates are crystalline, ice-like structures that consist of a guest molecules, such as methane or carbon dioxide, caged in a lattice of hydrogen-bonded water molecules.¹² An illustration of a methane gas hydrate structure I is given in Figure 1a. Approximately 160 m³ of methane can be stored in 1 m³ of hydrate, a significant increase in energy density.¹² Therefore, storing methane using gas hydrates is potentially quite favorable from an economic standpoint.

As for natural gas transport, the self-preservation kinetic anomaly observed in hydrates could be leveraged. S13 Gas hydrates typically form under high pressure and low temper-

Received: March 3, 2021 Revised: June 11, 2021 Published: June 28, 2021





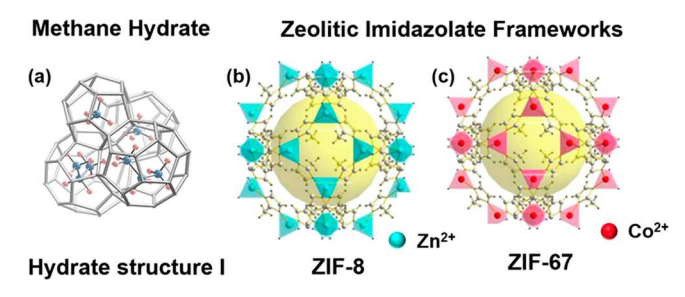


Figure 1. Illustration of (a) methane hydrate structure I with a unit cell size of 1.2 nm and the two zeolitic imidazolate frameworks of sodalite structures (b) ZIF-8 and (c) ZIF-67. The yellow spheres represent the internal pore, which has a diameter of 1.2 nm. 60,61 Not to scale.

ature conditions, and these conditions are specific to the type of guest molecule(s) present. Once the gas hydrate is formed, it can exhibit "self-preservation," a phenomenon in which a layer of ice forms around the hydrate particle and prevents gas from escaping the hydrate. After the ice layer is established, the pressure required to maintain a stable hydrate can be reduced to ambient pressure, so long as the temperature is kept below the freezing point of ice. Hydrates can be compressed to form a pellet with an ice layer, and they can then be transported at ambient pressure and low temperatures. Many studies in the literature have explored how long a hydrate is stable at ambient pressure conditions, with results ranging from 14 days at $-20~^{\circ}\mathrm{C}$ and 1 atm. 17 to 3 months at $-30~^{\circ}\mathrm{C}$ and 1 atm. 16

Several obstacles prevent the commercialization of hydrate technology. The two most significant barriers are long hydrate induction times and low water-to-hydrate conversion. Considerable effort has been dedicated to overcoming these issues. These efforts primarily target heat and mass transfer related solutions since hydrate growth is promoted when (1) the heat of hydrate formation is removed from the local formation area and (2) the mass transfer limitation of gas diffusion is reduced by increasing the gas-to-water contact area. Proposed avenues to these solutions include, but are not limited to, apparatus design, chemical additives, and porous materials. Some of the apparatus designs include stirred tank, 18 copper nanoparticles, 19 semicontinuous stirred tank; 20 water injection via spray nozzles;²¹ fixed bed reactor,²² and bubble column.²³ The chemical additives range from entirely inorganic to entirely organic, such as tetrahydrofuran (THF);²⁴ sodium dodecyl sulfate (SDS);²⁵ tetrabutylammonium bromide (TBAB);² tetrabutylammonium fluoride (TBAF);²⁷ cetyltrimethylammonium bromide (CTAB);¹⁹ methyl ester sulfonate;²⁸ and amino acids leucine, histidine, arginine, and tryptophan. 11,29

Porous materials provide a unique opportunity as they are also capable of storing methane in their frameworks via adsorption. By combining the methane storage capabilities of porous materials with gas hydrates, there can be a synergistic result where the amount stored with the combination of both hydrates and the porous materials is more than that of hydrates or porous materials on their own. The tested porous materials include macroporous, mesoporous, and microporous, such as silica sand; silica gels; slica gels; glass beads; activated carbon; clay; halloysite clay nanotubes; activated carbon; carbon nanotubes; carbon components from these overarching areas can be synergistic, as found in a study

by Inkong et al. that combined THF, hollow silica, and SDS^{50} and in a study by Wang et al. that coated graphene oxide nanosheets with $-SO_3$.

Metal-organic frameworks (MOFs) are a particularly interesting class of porous materials, as they are chemically diverse in composition, have large surface areas, and exhibit tunable porosity.⁵² As far as the authors are aware, the MOFs studied as methane hydrate promoters include MIL-53, 47 MIL-53(Al), ⁴⁵ ZIF-8, ^{30,45,46} HKUST-1, ^{45,49} MIL-101, ⁴⁸ MIL-100-(Fe), 46 Cr-soc-MOF-1, 31 and Y-shp-MOF-5. 31 These studies showed promising results for the application of MOFs as methane hydrate promoters, with more details of the results shown in Table S1. The studies on HKUST-1⁴⁹ and ZIF-8⁴⁶ reported high (>80%) water-to-hydrate conversion, whereas the other studies focused primarily on the amount of methane consumed by the hydrate and MOF. Of these studies, very few look at the recyclability and structural integrity of the metal organic frameworks after methane hydrate formation and dissociation, with the notable exceptions of two studies on ZIF-8^{45,46} and previous work by our group with HKUST-1.⁴⁹ Both ZIF-8 studies evaluated structural changes after only a single cycle of hydrate formation and dissociation, whereas our work with HKUST-1 evaluated these changes after three cycles. Therefore, more research is needed to determine the long-term viability of metal organic frameworks as methane hydrate promoters.

The porous materials relevant to this study are metal organic frameworks; more specifically, the materials are zeolitic imidazolate frameworks (ZIF), which is a subclass of MOFs. ZIFs contain both inorganic (metal ion) and organic (imidazolate linker) components, and the framework is composed of tetrahedral structural units, like that of zeolites.⁵ In this study, two microporous zeolitic imidazolate frameworks were chosen: ZIF-8 and ZIF-67. To the best of our knowledge, no studies have been documented on ZIF-67 as a methane hydrate promoter. Since these ZIFs are isostructural, the study of both would be helpful to better understand the role (if any) of the metal core in methane gas hydrate formation. ZIF-8 and ZIF-67 exhibit the same sodalite topology with imidazole linkers and zinc or cobalt metal centers, respectively.⁵⁴ Both ZIFs exhibit surface areas above 1000 m²/g, pore volumes of ca. 0.6 cm³/g, and internal pore diameters of 1.2 nm. ^{55–59} An illustration of the representative structures of ZIF-8 and ZIF-67 are given in Figure 1b and c, respectively.

For ZIF-8 and ZIF-67, the large surface areas and the internal pore diameter are advantageous for hydrate formation. The large surface area generates a large gas-to-water contact area, both externally and internally due to the pores. The diameter of the ZIFs cavity (1.2 nm) is approximately the same size of a methane hydrate structure I unit cell (1.2 nm), thus the pores could provide more interfacial area for gas hydrate formation. The confined space of the pore also can promote hydrate growth due to the pore's effect on the water activity, and this formation can act as a site for hydrate nucleation. ^{42,43}

These porous materials also have high methane adsorption capacity, with ZIF-8 reaching up to ~8 mmol/g at 80 bar, which provides a source of methane for hydrate formation. ^{45,62} The hydrophobicity of the ZIFs also plays an important role, as a hydrophobic surface positively affects the water ordering necessary for hydrate cages to begin to form. ⁶³ According to a study that tested the water stability of both ZIF-8 and ZIF-67, these ZIFs were stable in water to pressures as high as 800 bar, which indicates that these materials should maintain crystal

Table 1. Water-to-Hydrate Conversion, Dissociation Temperature, and Methane Stored Relative to the Amount of Water in the System for Four Water to Microporous Material Mass Ratios ($R_{\rm w}$) in the presence of ZIF-8 (Left) and ZIF-67 (Right), and without ZIFs⁴

ZIF-8				ZIF-67			
mass ratio H_2O to ZIF-8 (g/g)	conversion (%)	dissociation temperature (°C)	CH_4 stored to H_2O in system (mmol/g)	mass ratio H_2O to ZIF-67 (g/g)	conversion (%)	dissociation temperature (°C)	CH_4 stored to H_2O in system (mmol/g)
no ZIF-8	4.5	11.5	0.42	no ZIF-67	4.5	11.5	0.42
0.16	81.1	8.2	7.5	0.16	75.5	8.7	7.0
0.38	85.6	8.5	7.9	0.33	86.4	8.8	8.0
0.54	83.8	7.9	7.8	0.50	87.7	8.9	8.1
1.01	80.0	8.1	7.4	0.82	83.6	8.6	7.7

^aValues correspond to the third cycle of hydrate formation and dissociation.

integrity during and after the wet, high pressure environment in hydrate formation and dissociation experiments. ⁶⁴

In this study, the effect of ZIF-8 and ZIF-67 on methane hydrate growth was investigated using a high pressure differential scanning calorimeter (HP-DSC). Two key findings confirm that these microporous crystals are exceptional methane hydrate growth promoters displaying: (1) high water-to-hydrate conversion and (2) significant reduction in hydrate nucleation induction time. These encouraging results are most likely due to the ZIFs' large surface areas, hydrophobicity, water stability, and mechanical stability.

EXPERIMENTAL METHODS

ZIF-8 and ZIF-67 Materials and Synthesis Procedure. ZIF-8 and ZIF-67 were synthesized via microwave heating. This method has been employed for synthesis as it produces small crystals with a narrow size distribution, as observed in studies that used this method to synthesize other porous crystals, such as MOFs, 65,666 zeolites, 67 oxides, 68 and porous organic cages. 69

The procedure for synthesizing ZIF-8 is adapted from elsewhere. First, 0.10 g of zinc acetate hexahydrate (Sigma-Aldrich, >98%) was dissolved in 10 g of deionized water. Next, 0.41 g of 2-methylimidazolate (Aldrich, 99%) was added to the solution, which was stirred for 1 h. The resulting solution was put in a 100 cm³ Teflon-lined XP1500 vessel with a thermocouple inside. The vessel was then placed in a CEM Mars 5 microwave and heated to 120 °C for 30 min with a ramp time of 5 min at 100% of 400 W power, with a ramp time of 5 min. Once the vessel cooled naturally to room temperature, the solution was washed with deionized water and ethanol via centrifugation for 5 min at 3800 rpm. The resulting crystals were dried at 80 °C for 24 h.

The procedure for synthesizing ZIF-67 is similar to that of ZIF-8, with modifications from elsewhere. The precursors employed to synthesize ZIF-67 are 2-methylimidazolate (Aldrich, 99%), cobalt(II) nitrate hexahydrate (Sigma-Aldrich, >98%), and deionized water. First, 5.50 g of 2-methylimidazolate was dissolved into 20 g of deionized water. Second, in a separate beaker, 0.45 g of cobalt(II) nitrate hexahydrate was dissolved in 3 g of deionized water. Next, the two solutions were mixed together for 1 h. The combined solution was put in a 100 cm³ Teflon-lined XP1500 vessel with a thermocouple inside. The vessel was then placed in a CEM Mars 5 microwave and heated to 120 °C for 30 min at 100% of 400 W power, with a ramp time of 5 min. Once the vessel cooled naturally to room temperature, the solution was washed with deionized water and methanol via centrifugation for 5 min at 3800 rpm. The resulting crystals were dried at 80 °C for 24 h.

ZIF-8 and ZIF-67 Characterization Methods. To test the structural integrity of ZIF-8 and ZIF-67 crystals, a baseline was taken before subjecting the materials to the formation and dissociation of gas hydrates, and then one was taken after. To this end, a Siemens Kristalloflex 810 X-ray diffractometer was used to gather powder X-ray diffraction patterns of the microporous crystals. The diffractometer used Cu K α radiation operating at a wavelength of 1.54059 Å,

accompanied by a current of 25 mA and a voltage of 30 kV. The morphology of each material before and after hydrate formation and dissociation was inspected using a JEOL JSM-7000F field emission scanning electron microscope. An ASAP 2020 porosimeter (Micromeritics, Norcross, GA, USA) was used to collect nitrogen isotherms at $-196\,^{\circ}\mathrm{C}$, after the sample was degassed for 8 h at 200 $^{\circ}\mathrm{C}$ under a vacuum. Surface areas were calculated using the Brunauer–Emmet–Teller (BET) method following the criterion described by Rouquerol et al. 71 Pore size distributions were calculated using nonlocal density functional theory (NLDFT) for nitrogen on carbon slit pores. Pore volumes were calculated at P/Po = 0.9. Methane isotherms were collected at 0 $^{\circ}\mathrm{C}$ using the same ASAP 2020 porosimeter and employing similar degas conditions as the nitrogen isotherms.

High Pressure Differential Scanning Calorimeter Measurements. A high pressure differential scanning calorimeter (HP-DSC) VIIa from Seteram Inc. was used to investigate hydrate formation and dissociation. The HP-DSC operated within these criteria: a resolution of $0.04 \ \mu W$; a temperature range of -45 to $120 \ ^{\circ}C$ with a precision of $\pm 0.2 \ ^{\circ}C$; and a pressure range of 0.1-15.4 MPa, with a precision of ± 25 kPa. The schematic of the HP-DSC is given in Figure S1.

The employed methods are similar to our previous work.⁴⁹ Each sample was prepared by loading the cuvette HP-DSC cell with a specified amount of deionized water and then adding the dry crystalline material. The ratio of the water's mass relative to the material's mass is denoted by $R_{\rm w}$ and shown in the following equation:

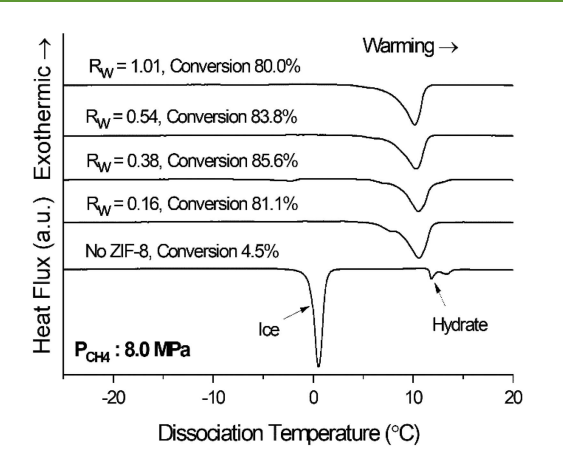
$$R_{\rm w} = \frac{\text{mass of water}}{\text{mass of ZIF}} \tag{1}$$

The sample was loaded into the HP-DSC and then pressurized with methane gas (Matherson, 99.99%). Two procedures were used for this research: scanning and isothermal. Each procedure was conducted at 8.0 MPa. Note that all of the HP-DSC experiments are performed *in situ*.

The scanning procedure started by raising the temperature of the system to 30 °C at a rate of 0.5 °C/min. The system was held at 30 °C for 3 h. Next, the system was cooled at a rate of 0.3 °C/min to -30 °C, then immediately warmed to 30 °C at a rate of 0.3 °C/min. To ensure reproducibility and crystal structure integrity, the cooling and heating process was repeated twice more, for a total of three times.

The isothermal procedure started by raising the temperature of the system to 30 $^{\circ}$ C at a rate of 0.5 $^{\circ}$ C/min. The system was held at 30 $^{\circ}$ C for 3 h. Next, the system was cooled at a rate of 0.8 $^{\circ}$ C/min to -15 $^{\circ}$ C, then held at that temperature for 24 h. Then, the system was warmed back up to 30 $^{\circ}$ C at a rate of 0.3 $^{\circ}$ C/min. This process was repeated once, for a total of two times.

For both the scanning and isothermal experiments, the heat flux profiles generated by the HP-DSC were collected. The appearance of peaks corresponded to either ice or hydrate formation or dissociation. The peak location indicates the time and temperature for hydrate formation/dissociation. The area under the peaks corresponds to the magnitude of the amount of hydrate and/or ice formed/dissociated in the system.



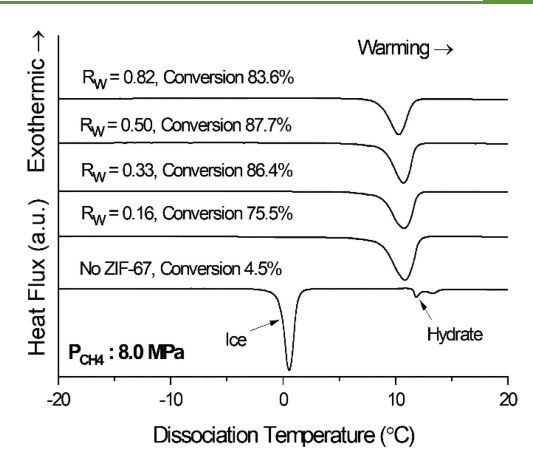


Figure 2. Warming HP-DSC heat flux profiles for ZIF-8 (left) and ZIF-67 (right), with respective values for crystal to water mass ratio ($R_{\rm w}$) and water-to-hydrate conversion conducted at 8.0 MPa.

Water-to-Hydrate Conversion Calculation. The water-to-hydrate conversion in the HP-DSC system was calculated via the following equation: ^{49,72}

hydrate conversion (%) = 100 ×
$$\frac{H_{\rm diss} \times {\rm MW}_{\rm H_2O} \times n_{\rm HYD}}{H_{\rm HYD}}$$
 (2)

 $H_{\rm diss}$ is the heat flux for the hydrate dissociation endothermic peak, as measured by the HP-DSC. $MW_{\rm H_2O}$ is the molecular weight of water (18 g/mol). $n_{\rm HYD}$ is the hydration number (5.9). 72 $H_{\rm HYD}$ is the known value of the heat of dissociation for a methane structure I hydrate (54.4 kJ/mol). 73

■ RESULTS AND DISCUSSION

Influence of ZIF-8 and ZIF-67 on Water-to-Hydrate Conversion. The zeolitic imidazolate frameworks ZIF-8 and ZIF-67 displayed remarkable performance as methane hydrate growth promoters. The measurements and calculations from the high pressure differential pressure scanning calorimeter (HP-DSC) experiments for a system with only water and with four systems with different water to microporous material mass ratios (R_w) are summarized in Table 1.

The warming heat flux profiles for these experiments are given in Figure 2. Full cooling and warming heat flux profiles for ZIF-8 and ZIF-67 are given in Figure S2, with the corresponding temperature profile of the HP-DSC system overlaid.

The addition of either ZIF-8 or ZIF-67 dramatically increased water-to-hydrate conversion as compared to a system without any porous material. The water-to-hydrate conversion ranged from 80.0 to 85.6% for ZIF-8 and from 75.5 to 87.7% for ZIF-67 for different water to ZIF mass ratios. A system with ZIF-8 increased the water-to-hydrate conversion by as much as 15.3 times, raising it from 4.5% to 85.6%. A system with ZIF-67 increased water-to-hydrate conversion by as much as 15.7 times, from 4.5% to 87.7%. Therefore, the addition of ZIF-8 and ZIF-67 increased the amount of methane stored relative to the amount of water in the system from 0.42 mmol/g to highs of 7.9 mmol/g and 8.1 mmol/g, respectively. The amount of methane stored accounts only for the amount that is captured in the hydrate as determined using the methane structure I hydration number and heat flux from the respective HP-DSC experiments and does not include the amount of methane potentially adsorbed on the microporous crystal.

The high water-to-hydrate conversion seen in this study most likely stems from physical and chemical properties of the two ZIFs. The high surface area of ZIF-8 ($1052~\text{m}^2/\text{g}$) and ZIF-67 ($1585~\text{m}^2/\text{g}$) increased the gas-to-water contact area, thus reducing the gas diffusion barrier caused by a hydrate growth forming a film at the interface of gas and water. The water-to-hydrate conversion of neither ZIF-8 nor ZIF-67 exhibited a significant dependency on the crystal-to-water mass ratio. A small decrease in conversion was observed at the highest studied ZIF to water mass ratio of 1.01, most likely due to the increased amount of water slightly decreasing the gas-to-water contact area.

The organic linker 2-methylimidazole, present in both ZIF-8 and ZIF-67, contributes to high hydrophobicity in both materials, as evident from water contact angle measurements and water adsorption isotherms reported in the literature. 58,59,74-76 This high hydrophobicity promotes hydrate growth, as found by a study that compared the efficacy of a hydrophobic and a hydrophilic MOF in promoting methane hydrate growth. These authors demonstrated that the hydrophobic MOF promoted more water-to-hydrate conversion, thus increasing the amount of methane stored in hydrate form. Other studies in the literature determined that a hydrophobic surface does not negatively interfere with the ordering of water molecules necessary for hydrate nucleation, Tr.78 further supporting the positive effect of hydrophobicity in hydrate growth.

Another influential property of ZIF-8 and ZIF-67 is their relatively high methane adsorption. The methane adsorption isotherms obtained for the synthesized ZIF-8 and ZIF-67 are shown in Figure S3. The linear shape of the methane adsorption isotherms collected in this work are at low pressures (max of 1.1 bar) and match the shape of methane adsorption for both ZIF-8 and ZIF-67 at these similar low pressures. 46,62 ZIF-8 stores approximately 0.33 mmol CH₄/g at 1 bar and 273 K, which is less than the value reported in the literature under similar conditions (0.53 mmol/g at 1 bar and 273 K).⁶² The difference in CH₄ uptake may be related to different textural and morphological properties (surface area, crystal size among others). ZIF-67 stored more than ZIF-8, reaching a high of 0.41 mmol CH₄/g at 1 bar and 273 K. This value, as well, was lower than reported in the literature (0.54 mmol/g at 1 bar and 273 K).⁶² Note, at higher pressures (~80 bar), studies observed significantly higher methane adsorption (~8 mmol/g) for ZIF-8, thus more methane may be adsorbed to the ZIFs at the conditions of the HP-DSC.⁴⁵ The methane adsorbed on the material's surface acted as a methane source for hydrate formation. When combined with the hydrophobicity of the materials, this methane source helps promote hydrate growth, as observed in a similar system with silica material.

An isothermal HP-DSC elucidated that ZIF-8 and ZIF-67 dramatically reduced the hydrate nucleation induction time (i.e., the time between the system's stabilization at $-15\,^{\circ}\mathrm{C}$ and the appearance of an exothermic peak, which is indicative of hydrate formation). A system with no porous material had a nucleation induction time of 3.8 \pm 1.3 h. ZIF-8 and ZIF-67 reduced this time on average by 2.0 h (51.6% decrease) and 3.5 h (92.2% decrease), respectively. Therefore, these materials provide a considerable kinetic advantage as methane hydrate promoters. Figure 3 shows the isothermal HP-DSC profiles of ZIF-8 and ZIF-67 compared to a system without any material.

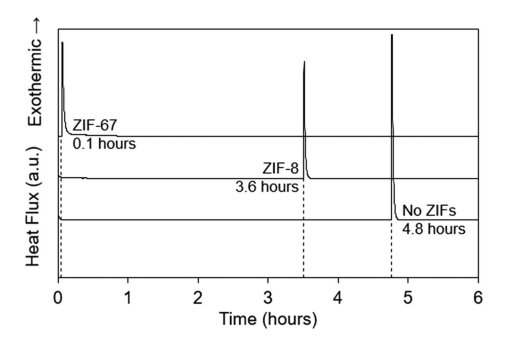


Figure 3. Profile of isothermal HP-DSC experiments conducted at -15 °C for ZIF-67 (top), ZIF-8 (middle), and a system without any porous material (bottom). The exothermic peaks correspond to the heat released from hydrate formation.

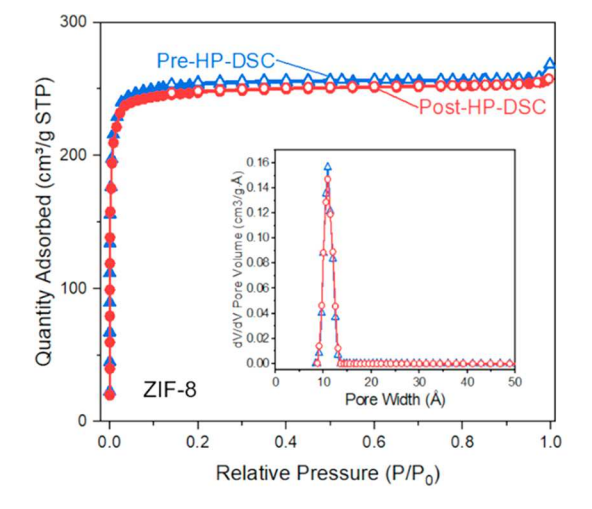
In terms of shortening hydrate nucleation induction time, ZIF-67 exceeded the performance of ZIF-8. The 1.3-h-faster induction time of ZIF-67 can be attributed to two measured properties that differ between the synthesized ZIFs: surface area and methane adsorption. The synthesized ZIF-67 has a surface area of 1585 $\rm m^2/g$, whereas the surface area of the synthesized ZIF-8 is 1052 $\rm m^2/g$. As mentioned above, the methane adsorption of ZIF-67 (0.41 mmol/g at 1 bar) is

higher than ZIF-8 (0.33 mmol/g at 1 bar). For both materials, methane adsorbs preferentially to the organic linker, not the metal ions. The larger surface area is capable of containing more adsorbed methane, and thus surface area is the primary reason for differing induction times. Therefore, the higher surface area and methane adsorption capacity of ZIF-67 results in ZIF-67 reducing the hydrate nucleation induction time more than ZIF-8.

Effect of ZIF-8 and ZIF-67 on Hydrate Dissociation Temperature. The average hydrate dissociation temperatures in systems with ZIF-8 (8.2 °C \pm 0.3) or ZIF-67 (8.8 °C \pm 0.1) are notably lower than that in a system without any porous material (11.5 °C \pm 0.1). (These data are also shown in Table 1.) The shift to a lower hydrate dissociation temperature is indicative of hydrate formation inside the material, rather than just on the external surface. The depression in the dissociation temperature is caused by confined water molecules in the pores having lower water activity. 47,83

The low water activity requires more thermodynamic driving force to form stable hydrates, and thus these hydrates dissociate at lower temperatures when compared to a bulk hydrate system. Typically, the extent of depression of the hydrate dissociation temperature depends upon the size of the pores, with smaller pore sizes (not smaller than the unit cell size of a hydrate) resulting in a greater depression. Thus, methane hydrate formation is taking place in a confined space provided by the ZIFs. The first possible confined space is the pores, as nitrogen isotherms of ZIF-8 and ZIF-67, shown in Figure 4, reveal that, for both materials, the larger pore cavity width is ~1.2 nm, which is about the size of the structure I hydrate unit cell (1.2 nm). Additionally, the organic linkers in the ZIFs' structure leads to flexibility and thus could expand to better accommodate a methane hydrate.

Although possible, the pores are an unlikely location for hydrate formation due to the similarities in pore size and the hydrophobic nature of the ZIFs. Even though the hydrophobic external surface of ZIF-8 and ZIF-67 promotes hydrate growth through its positive effect on water ordering, the hydrophobicity limits water uptake into the crystal structure. Water adsorption isotherms reported for ZIF-8 and ZIF-67 in the literature show low water uptake, in the range of 0.2 mmol/g to 0.5 mmol/g depending upon the relative pressure. 75,76 The



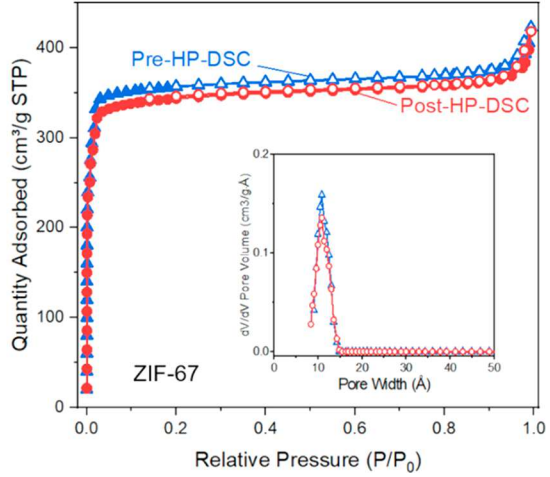


Figure 4. Nitrogen isotherms with insets showing pore distributions calculated from NLDFT for synthesized ZIF-8 (left) and ZIF-67 (right) before and after subjecting the crystals to hydrate formation (pre HP-DSC) and hydrate dissociation (post HP-DSC).

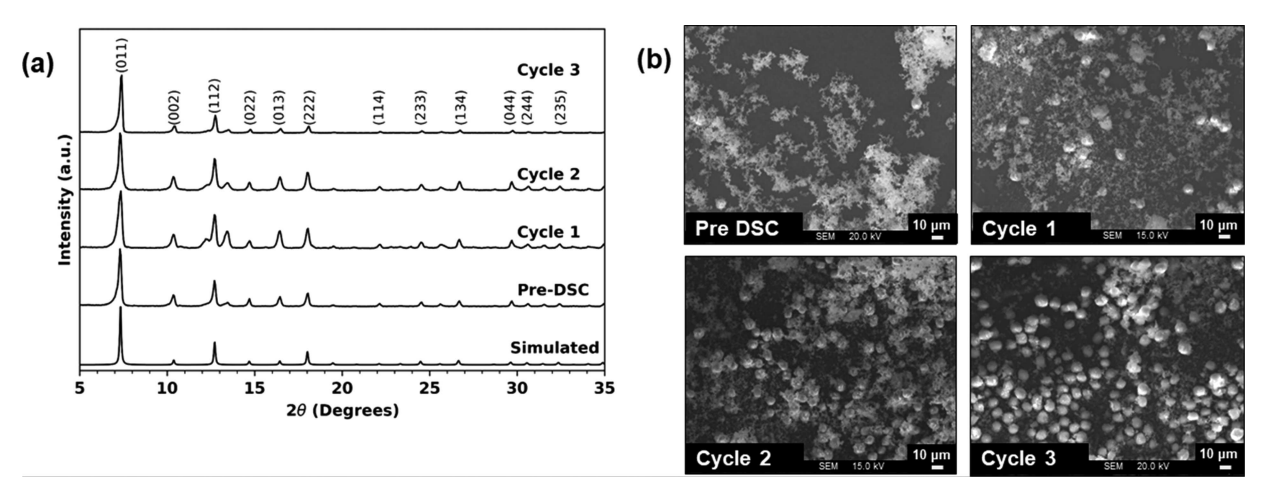


Figure 5. (a) X-ray diffraction patterns of the ZIF-8 sample before hydrate formation and dissociation (Pre-DSC), the ZIF-8 sample after three consecutive cycles, and a simulated pattern for ZIF-8. (b) SEM images of the ZIF-8 sample before the HP-DSC and then after three consecutive cycles.

flexible structure of the ZIFs does exhibit better diffusion of molecules at high pressure, such as the conditions in the HP-DSC. An experimental and simulation study on ZIF-8 at high pressures found that at high pressures, the pore windows (3.4 Å) expanded to allow transport of molecules through it that typically were too large to fit, such as methane (3.8 Å), a phenomenon termed "gate opening." The enlargement accounts for the high methane adsorption capacity of ZIF-8 at high pressures ranging from 1.8 mmol/g at 1 MPa to 8.5 mmol/g at 10 MPa. 45,85,86 The gate opening of the ZIFs at high pressure thus would allow more diffusion of water throughout the structure, potentially giving rise to hydrate formation within the ZIFs pores. The hydrate formed may only be defective hydrate crystals, a result found in a study that used inelastic neutron scattering to observe hydrate formation in the micropores (<0.7 nm) of hydrophobic activated carbon.³⁹

Most likely, though, the reduced dissociation temperature observed in this study with ZIF-8 and ZIF-67 results from formation in the interstitial spacing rather than the pores. This interstitial space is formed of the gaps that result from uneven packing of crystallites in a ZIF particle. A study on MIL-53 found that the hydrate dissociation temperature decreased in the presence of MIL-53, yet the micropore of MIL-53 (0.6 nm) are too small for the structure I unit hydrate cell. It has been suggested that the observed depression in the hydrate dissociation temperature was caused by hydrate formation taking place in the interstitial space. Therefore, if the interstitial spacing is significant, then it may act more like an external surface and would not significantly inhibit the water diffusion necessary to form hydrates within these spaces.

Characterization of ZIF-8 Pre- and Post-Hydrate Formation and Dissociation. With regard to water-to-hydrate conversion, ZIF-8 exhibited a unique trend over the first three cycles of hydrate formation and dissociation. Conversion increased from 51.3% in the first cycle to 78.6% in the second and 85.6% in the third. After the third cycle, the consecutive fourth and fifth cycles only showed deviations of ±2.7% from the third cycle. These stabilized results indicate that a change in the material occurred within the first three cycles. Figure 5a shows the powder X-ray diffraction (XRD) patterns of ZIF-8 pre- and post-HP-DSC, showing a good match to the simulated sodalite crystallographic pattern, and

the relative crystallinity of the peak at 7.3 2θ was maintained with only a 2% deviation over all the cycles.

Notably, however, an unexpected peak arose after the first cycle at 13.4 2θ . This peak then decreased in intensity and nearly disappeared by the third cycle. The presence of this peak may be related to a change in surface morphology.

The SEM images in Figure 5b confirm that a morphological change took place after each of the first three cycles. The original ZIF-8 sample was a fine powder with an average crystal size of 1.05 \pm 0.09 μ m. After the first cycle, large crystal agglomerates started to appear. Magnified SEM images, shown in Figure S4, suggest that the agglomerates arise from the merging of the small crystal particles, as evident in the dashed red circles on the images. Immediately after the first cycle, these agglomerates measured up to 8.89 \pm 1.10 μ m, while the other crystals maintained a size of 1.13 \pm 0.17 $\mu \mathrm{m}.$ The ratio of agglomerates to original particles increased with each cycle until almost all of the small crystals were agglomerated. This increase in agglomeration correlated to an increase in conversion, as depicted in Figure S5. Therefore, the process of hydrate formation and dissociation must cause the agglomeration; the agglomeration, in turn, promotes more hydrate growth.

Agglomeration of the ZIF-8 particles was observed in another study that examined the performance of ZIF-8 as a promoter.³⁰ The authors only conducted one cycle of hydrate formation and dissociation, but they found that as the water content in their test increased, the extent of agglomeration increased, too. Therefore, they concluded that water caused ZIF-8 to agglomerate due to the strong hydrogen bonds formed by water molecules making the ZIF-8 particles more attracted to one another.³⁰ According to the literature, ZIF-8 does not experience any deformation upon exposure to high pressure methane⁴⁶—thus eliminating high pressure as a potential cause of agglomeration. Hence, the observed increase of agglomeration is most likely attributable to increased time of water exposure, with which it correlates.

Another study that used ZIF-8 as a methane hydrate promoter found that the behavior of the porous material changed after a single cycle of formation and dissociation. The authors concluded that, during the first cycle, hydrate formation takes place primarily in the pores of the ZIF-8 crystal structure, whereas in the second cycle, hydrate

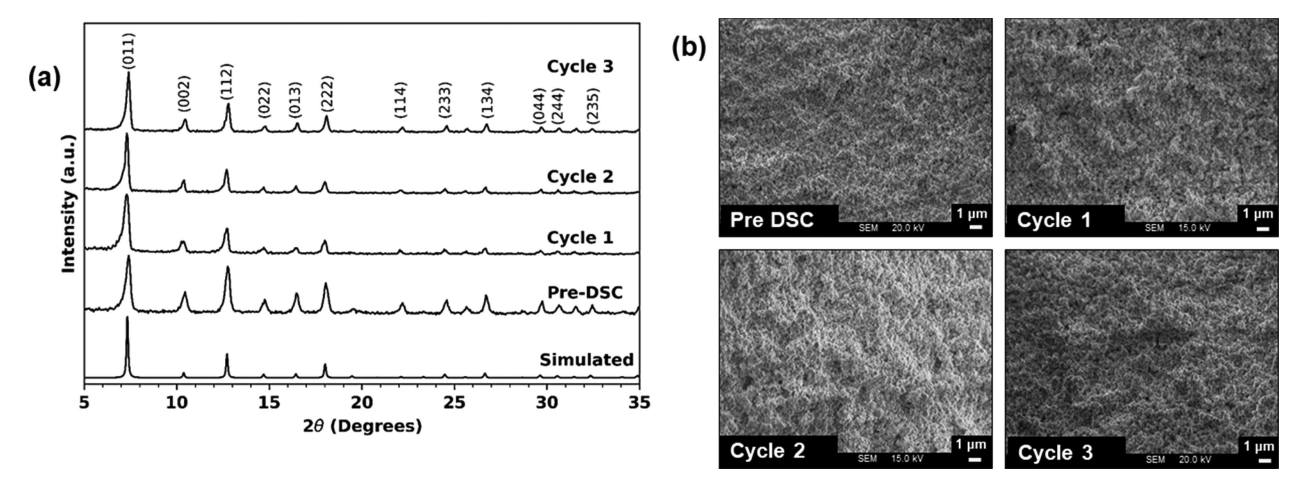


Figure 6. (a) X-ray diffraction patterns of the ZIF-67 sample before hydrate formation and dissociation (Pre-DSC), the ZIF-67 sample after three consecutive cycles, and a simulated pattern for ZIF-67. (b) SEM images of the ZIF-67 sample before the HP-DSC and then after three consecutive cycles.

formation occurs in the interstitial space between crystals or on the external surface. The ZIF-8 agglomerates in this study may be forming optimal interstitial spacing for hydrate formation as the single crystals merge. Interestingly, the agglomeration of ZIF-8 particles did not significantly affect surface area (1052 m²/g to 1031 m²/g) or pore volume (0.4 cm³/g to 0.39 cm³/g). Other than the observed morphology change, the integrity of the ZIF-8 structure is maintained.

Characterization of ZIF-67 Pre- and Post-Hydrate Formation and Dissociation. For ZIF-67, water-to-hydrate conversion remained consistent throughout each hydrate formation and dissociation cycle. The XRD pattern of the Pre-DSC sample of ZIF-67 matched the simulated sodalite pattern well, as shown in Figure 5a.

No appreciable changes occurred in the XRD pattern between the pre- and post-DSC samples aside from an increase in relative crystallinity of the peak at 7.3 2θ after the first cycle of hydrate formation and dissociation. The ~30% observed increase after the first cycle can be attributed to the HP-DSC conditions interacting with any unused precursors to complete the crystal synthesis, a phenomenon observed in a study on the effect of ZIF-67 synthesis time on relative crystallinity.⁸⁷ To ensure no further changes occurred, a sample of ZIF-67 after eight cycles was compared to the sample after one cycle, and the crystallinity only differed by ±1%. Figure 5b shows SEM images of the ZIF-67 sample before and after hydrate formation and dissociation. The ZIF-67 crystals as synthesized were packed together but did not agglomerate after each cycle. Magnified SEM images of the surface morphology of the ZIF-67, shown in Figure S6, further indicate that no morphology changes occurred. The consistency of hydrate conversion and the absence of significant changes in the XRD patterns or SEM images of the pre- and post-DSC ZIF-67 samples indicate that ZIF-67 preserved its structural integrity and resulted in outstanding recyclability. A brief investigation was conducted on the particle size effect for ZIF-67 on hydrate growth promotion. The small particles (0.21 \pm 0.05 μ m), shown in Figure 6, led to a conversion of 87.7% at an R_w of 0.50, as reported in Table 1. Interestingly, when larger size ZIF-67 particles (2.95 \pm 0.45 μ m), shown in Figure S7, were subjected to the HP-DSC, the conversion was 87.6% at an $R_{\rm w}$ of 0.57. This indicates that for ZIF-67 the particle size does not play a significant role in the hydrate growth promotion performance.

While the water-to-hydrate conversion for both ZIFs was similar, there was a difference in the methane hydrate nucleation induction time between the two ZIFs. The difference in reduction observed with ZIF-67 relative to ZIF-8 stems from higher methane adsorption of ZIF-67 as compared to ZIF-8 (0.41 mmol/g versus 0.33 mmol/g, respectively). Since both ZIFs are isostructural and have the same linker, this difference in adsorption uptake is related to the presence of different metal cores and different textural properties of both ZIFs.

■ CONCLUSIONS

The methane hydrate growth promotion performance of the two studied zeolitic imidazolate frameworks, ZIF-8 and ZIF-67, showed highly promising results, with water-to-hydrate conversions as high as 85.6% and 87.7%, respectively. The primary factor was the large surface area of ZIF-8 ($1052 \text{ m}^2/\text{g}$) and ZIF-67 (1585 m²/g) reducing mass transport limitations by increasing the gas-to-water contact area. ZIF-8 and ZIF-67 reduced the induction times on average by 51.6% and 92.2%, respectively. The difference in reduction observed with ZIF-67 relative to ZIF-8 stems from higher methane adsorption of ZIF-67 as compared to ZIF-8 (0.41 mmol/g versus 0.33 mmol/g at 1 bar, respectively). ZIF-8 experienced a morphological change over the course of three consecutive cycles of hydrate formation and dissociation while maintaining crystallinity. The fourth and fifth cycle resulted in consistent conversion to the third cycle, and the morphological changes to ZIF-8 ceased after the third cycle, indicating that these two were correlated. The structural integrity of both ZIFs was preserved. The results from this study conclude that ZIF-8 and ZIF-67 are highly suitable methane hydrate growth promoters. This work demonstrates that ZIF-8 and ZIF-67 are capable of overcoming the mass transfer limitations and slow kinetics typical of methane hydrate formation, exhibiting exceptional potential as a way to transition methane hydrates into an efficient and economical method for methane storage and transportation.

ASSOCIATED CONTENT

Supporting Information

The Supporting Information is available free of charge at https://pubs.acs.org/doi/10.1021/acssuschemeng.1c01488.

Table summarizing literature review of MOFs as methane hydrate growth promoters, schematic of the high pressure differential scanning calorimeter (HP-DSC), full HP-DSC cooling and warming profiles, methane adsorption isotherms, water-to-hydrate conversion for three cycles of ZIF-8 (PDF)

AUTHOR INFORMATION

Corresponding Authors

Carolyn A. Koh — Chemical and Biological Engineering Department, Colorado School of Mines, Golden, Colorado 80401, United States; orcid.org/0000-0003-3452-4032; Email: ckoh@mines.edu

Moises A. Carreon — Chemical and Biological Engineering Department, Colorado School of Mines, Golden, Colorado 80401, United States; orcid.org/0000-0001-6391-2478; Email: mcarreon@mines.edu

Authors

Shurraya Denning — Chemical and Biological Engineering Department, Colorado School of Mines, Golden, Colorado 80401, United States

Ahmad A. A. Majid — Chemical and Biological Engineering Department, Colorado School of Mines, Golden, Colorado 80401, United States

Jolie M. Lucero — Chemical and Biological Engineering Department, Colorado School of Mines, Golden, Colorado 80401, United States; orcid.org/0000-0002-4606-7118

James M. Crawford — Chemical and Biological Engineering Department, Colorado School of Mines, Golden, Colorado 80401, United States; orcid.org/0000-0003-3614-6055

Complete contact information is available at: https://pubs.acs.org/10.1021/acssuschemeng.1c01488

Notes

The authors declare no competing financial interest.

ACKNOWLEDGMENTS

Financial support from the National Science Foundation (CBET award # 1835924) is gratefully acknowledged.

REFERENCES

- (1) U.S. Energy Information Administration. *International Energy Outlook* 2020; U.S. Energy Information Administration, 2020.
- (2) Yeon, S. H.; Seol, J.; Koh, D. Y.; Seo, Y. J.; Park, K. P.; Huh, D. G.; Lee, J.; Lee, H. Abnormal Methane Occupancy of Natural Gas Hydrates in Deep Sea Floor Sediments. *Energy Environ. Sci.* **2011**, *4* (2), 421–424.
- (3) Boswell, R.; Collett, T. S. Current Perspectives on Gas Hydrate Resources. *Energy Environ. Sci.* **2011**, *4*, 1206–1215.
- (4) Huang, K.; Miller, J. B.; Huber, G. W.; Dumesic, J. A.; Maravelias, C. T. A General Framework for the Evaluation of Direct Nonoxidative Methane Conversion Strategies. *Joule* **2018**, 2 (2), 349–365.
- (5) Chong, Z. R.; Yang, S. H. B.; Babu, P.; Linga, P.; Li, X.-S. Review of Natural Gas Hydrates as an Energy Resource: Prospects and Challenges. *Appl. Energy* **2016**, *162*, 1633–1652.
- (6) Sloan, E. D. Fundamental Principles and Applications of Natural Gas Hydrates. *Nature* **2003**, *426*, 353–359.
- (7) Bhattacharjee, G.; Goh, M. N.; Arumuganainar, S. E. K.; Zhang, Y.; Linga, P. Ultra-Rapid Uptake and the Highly Stable Storage of Methane as Combustible Ice †. *Energy Environ. Sci.* **2020**, *13*, 4946.
- (8) Wilmer, C. E.; Farha, O. K.; Yildirim, T.; Eryazici, I.; Krungleviciute, V.; Sarjeant, A. A.; Snurr, R. Q.; Hupp, J. T. Gram-

- Scale, High-Yield Synthesis of a Robust Metal-Organic Framework for Storing Methane and Other Gases. *Energy Environ. Sci.* **2013**, 6 (4), 1158–1163.
- (9) Marco-Lozar, J. P.; Kunowsky, M.; Suárez-García, F.; Carruthers, J. D.; Linares-Solano, A. Activated Carbon Monoliths for Gas Storage at Room Temperature. *Energy Environ. Sci.* **2012**, *5* (12), 9833–9842.
- (10) Li, B.; Wen, H. M.; Wang, H.; Wu, H.; Yildirim, T.; Zhou, W.; Chen, B. Porous Metal-Organic Frameworks with Lewis Basic Nitrogen Sites for High-Capacity Methane Storage. *Energy Environ. Sci.* **2015**, 8 (8), 2504–2511.
- (11) Veluswamy, H. P.; Kumar, A.; Kumar, R.; Linga, P. An Innovative Approach to Enhance Methane Hydrate Formation Kinetics with Leucine for Energy Storage Application. *Appl. Energy* **2017**, *188*, 190–199.
- (12) Sloan, E. D.; Koh, C. A. Clathrate Hydrates of Natural Gases, 3rd ed.; CRC Press: New York, 2008.
- (13) Khurana, M.; Yin, Z.; Linga, P. A Review of Clathrate Hydrate Nucleation. ACS Sustainable Chem. Eng. 2017, 5, 11176–11203.
- (14) Stern, L. A.; Circone, S.; Kirby, S. H.; Durham, W. B. Anomalous Preservation of Pure Methane Hydrate at 1 Atm. *J. Phys. Chem. B* **2001**, *105* (9), 1756–1762.
- (15) Veluswamy, H. P.; Kumar, A.; Seo, Y.; Lee, J. D.; Linga, P. A Review of Solidified Natural Gas (SNG) Technology for Gas Storage via Clathrate Hydrates. *Appl. Energy* **2018**, *216*, 262–285.
- (16) Mimachi, H.; Takahashi, M.; Takeya, S.; Gotoh, Y.; Yoneyama, A.; Hyodo, K.; Takeda, T.; Murayama, T. Effect of Long-Term Storage and Thermal History on the Gas Content of Natural Gas Hydrate Pellets under Ambient Pressure. *Energy Fuels* **2015**, 29 (8), 4827–4834.
- (17) Mimachi, H.; Takeya, S.; Yoneyama, A.; Hyodo, K.; Takeda, T.; Gotoh, Y.; Murayama, T. Natural Gas Storage and Transportation within Gas Hydrate of Smaller Particle: Size Dependence of Self-Preservation Phenomenon of Natural Gas Hydrate. *Chem. Eng. Sci.* **2014**, *118*, 208–213.
- (18) Lee, J. M.; Cho, S. J.; Lee, J. D.; Linga, P.; Kang, K. C.; Lee, J. Insights into the Kinetics of Methane Hydrate Formation in a Stirred Tank Reactor by In Situ Raman Spectroscopy. *Energy Technol.* **2015**, 3 (9), 925–934.
- (19) Pahlavanzadeh, H.; Rezaei, S.; Khanlarkhani, M.; Manteghian, M.; Mohammadi, A. H. Kinetic Study of Methane Hydrate Formation in the Presence of Copper Nanoparticles and CTAB. *J. Nat. Gas Sci. Eng.* **2016**, *34*, 803–810.
- (20) Hao, W.; Wang, J.; Fan, S.; Hao, W. Study on Methane Hydration Process in a Semi-Continuous Stirred Tank Reactor. *Energy Convers. Manage.* **2007**, *48* (3), 954–960.
- (21) Rossi, F.; Filipponi, M.; Castellani, B. Investigation on a Novel Reactor for Gas Hydrate Production. *Appl. Energy* **2012**, *99*, 167–172.
- (22) Filarsky, F.; Schmuck, C.; Schultz, H. J. Impact of Modified Silica Beads on Methane Hydrate Formation in a Fixed-Bed Reactor. *Ind. Eng. Chem. Res.* **2019**, *58* (36), 16687–16695.
- (23) Luo, Y. T.; Zhu, J. H.; Fan, S. S.; Chen, G. J. Study on the Kinetics of Hydrate Formation in a Bubble Column. *Chem. Eng. Sci.* **2007**, *62* (4), 1000–1009.
- (24) Veluswamy, H. P.; Wong, A. J. H.; Babu, P.; Kumar, R.; Kulprathipanja, S.; Rangsunvigit, P.; Linga, P. Rapid Methane Hydrate Formation to Develop a Cost Effective Large Scale Energy Storage System. *Chem. Eng. J.* **2016**, *290*, 161–173.
- (25) Zhang, J. S.; Lee, S.; Lee, J. W. Kinetics of Methane Hydrate Formation from SDS Solution. *Ind. Eng. Chem. Res.* **2007**, *46* (19), 6353–6359.
- (26) Zhong, D.; Englezos, P. Methane Separation from Coal Mine Methane Gas by Tetra-n-Butyl Ammonium Bromide Semiclathrate Hydrate Formation. *Energy Fuels* **2012**, *26* (4), 2098–2106.
- (27) Shi, L.; Liang, D. Semiclathrate Hydrate Phase Behaviour and Structure for CH4 in the Presence of Tetrabutylammonium Fluoride (TBAF). *J. Chem. Thermodyn.* **2019**, *135*, 252–259.
- (28) Inkong, K.; Veluswamy, H. P.; Rangsunvigit, P.; Kulprathipanja, S.; Linga, P. Investigation on the Kinetics of Methane Hydrate

- Formation in the Presence of Methyl Ester Sulfonate. J. Nat. Gas Sci. Eng. 2019, 71, 102999.
- (29) Veluswamy, H. P.; Lee, P. Y.; Premasinghe, K.; Linga, P. Effect of Biofriendly Amino Acids on the Kinetics of Methane Hydrate Formation and Dissociation. *Ind. Eng. Chem. Res.* **2017**, *56* (21), 6145–6154.
- (30) Mu, L.; Liu, B.; Liu, H.; Yang, Y.; Sun, C.; Chen, G. A Novel Method to Improve the Gas Storage Capacity of ZIF-8. *J. Mater. Chem.* **2012**, 22 (24), 12246–12252.
- (31) Cuadrado-Collados, C.; Mouchaham, G.; Daemen, L.; Cheng, Y.; Ramirez-Cuesta, A.; Aggarwal, H.; Missyul, A.; Eddaoudi, M.; Belmabkhout, Y.; Silvestre-Albero, J. Quest for an Optimal Methane Hydrate Formation in the Pores of Hydrolytically Stable Metal-Organic Frameworks. J. Am. Chem. Soc. 2020, 142 (31), 13391–13397.
- (32) Chong, Z. R.; Yang, M.; Khoo, B. C.; Linga, P. Size Effect of Porous Media on Methane Hydrate Formation and Dissociation in an Excess Gas Environment. *Ind. Eng. Chem. Res.* **2016**, *55* (29), 7981–7991.
- (33) Smith, D. H.; Wilder, J. W.; Seshadri, K. Methane Hydrate Equilibria in Silica Gels with Broad Pore-Size Distributions. *AIChE J.* **2002**, *48* (2), 393–400.
- (34) Fan, S.; Yang, L.; Lang, X.; Wang, Y.; Xie, D. Kinetics and Thermal Analysis of Methane Hydrate Formation in Aluminum Foam. *Chem. Eng. Sci.* **2012**, 82, 185–193.
- (35) Yang, L.; Fan, S.; Wang, Y.; Lang, X.; Xie, D. Accelerated Formation of Methane Hydrate in Aluminum Foam. *Ind. Eng. Chem. Res.* **2011**, *50* (20), 11563–11569.
- (36) Kumar, A.; Sakpal, T.; Roy, S.; Kumar, R. Methane Hydrate Formation in a Test Sediment of Sand and Clay at Various Levels of Water Saturation. *Can. J. Chem.* **2015**, 93 (8), 874–881.
- (37) Em, Y.; Stoporev, A.; Semenov, A.; Glotov, A.; Smirnova, E.; Villevald, G.; Vinokurov, V.; Manakov, A.; Lvov, Y. Methane Hydrate Formation in Halloysite Clay Nanotubes. *ACS Sustainable Chem. Eng.* **2020**, *8* (21), 7860–7868.
- (38) Cuadrado-Collados, C.; Fauth, F.; Such-Basañez, I.; Martínez-Escandell, M.; Silvestre-Albero, J. Methane Hydrate Formation in the Confined Nanospace of Activated Carbons in Seawater Environment. *Microporous Mesoporous Mater.* **2018**, 255, 220–225.
- (39) Cuadrado-Collados, C.; Majid, A. A. A.; Martínez-Escandell, M.; Daemen, L. L.; Missyul, A.; Koh, C.; Silvestre-Albero, J. Freezing/Melting of Water in the Confined Nanospace of Carbon Materials: Effect of an External Stimulus. *Carbon* **2020**, *158*, 346–355.
- (40) Pasieka, J.; Coulombe, S.; Servio, P. Investigating the Effects of Hydrophobic and Hydrophilic Multi-Wall Carbon Nanotubes on Methane Hydrate Growth Kinetics. *Chem. Eng. Sci.* **2013**, *104*, 998–1002
- (41) Zang, X.; Du, J.; Liang, D.; Fan, S.; Tang, C. Influence of A-Type Zeolite on Methane Hydrate Formation. *Chin. J. Chem. Eng.* **2009**, *17* (5), 854–859.
- (42) Zhao, Y.; Zhao, J.; Liang, W.; Gao, Q.; Yang, D. Semi-Clathrate Hydrate Process of Methane in Porous Media-Microporous Materials of SA-Type Zeolites. *Fuel* **2018**, 220, 185–191.
- (43) Andres-Garcia, E.; Dikhtiarenko, A.; Fauth, F.; Silvestre-Albero, J.; Ramos-Fernández, E. V.; Gascon, J.; Corma, A.; Kapteijn, F. Methane Hydrates: Nucleation in Microporous Materials. *Chem. Eng. J.* **2019**, *360*, *569*–*576*.
- (44) Kim, N.-J.; Park, S.-S.; Shin, S.-W.; Hyun, J.-H.; Chun, W. An Experimental Investigation into the Effects of Zeolites on the Formation of Methane Hydrates. *Int. J. Energy Res.* **2015**, 39 (1), 26–32.
- (45) Liu, H.; Zhan, S.; Guo, P.; Fan, S.; Zhang, S. Understanding the Characteristic of Methane Hydrate Equilibrium in Materials and Its Potential Application. *Chem. Eng. J.* **2018**, 349, 775–781.
- (46) Casco, M. E.; Rey, F.; Jordá, J. L.; Rudić, S.; Fauth, F.; Martínez-Escandell, M.; Rodríguez-Reinoso, F.; Ramos-Fernández, E. V.; Silvestre-Albero, J. Paving the Way for Methane Hydrate Formation on Metal-Organic Frameworks (MOFs). *Chem. Sci.* **2016**, 7 (6), 3658–3666.

- (47) Kim, D.; Ahn, Y. H.; Lee, H. Phase Equilibria of CO2 and CH4 Hydrates in Intergranular Meso/Macro Pores of MIL-53 Metal Organic Framework. *J. Chem. Eng. Data* **2015**, *60* (7), 2178–2185.
- (48) He, Z.; Zhang, K.; Jiang, J. Formation of CH4 Hydrate in a Mesoporous Metal-Organic Framework MIL-101: Mechanistic Insights from Microsecond Molecular Dynamics Simulations. *J. Phys. Chem. Lett.* **2019**, *10*, 7002–7008.
- (49) Denning, S.; Majid, A. A.; Lucero, J. M.; Crawford, J. M.; Carreon, M. A.; Koh, C. A. Metal—Organic Framework HKUST-1 Promotes Methane Hydrate Formation for Improved Gas Storage Capacity. ACS Appl. Mater. Interfaces 2020, 12, 53510.
- (50) Inkong, K.; Veluswamy, H. P.; Rangsunvigit, P.; Kulprathipanja, S.; Linga, P. Innovative Approach to Enhance the Methane Hydrate Formation at Near-Ambient Temperature and Moderate Pressure for Gas Storage Applications. *Ind. Eng. Chem. Res.* **2019**, 58 (49), 22178–22192.
- (51) Wang, F.; Meng, H. L.; Guo, G.; Luo, S. J.; Guo, R. B. Methane Hydrate Formation Promoted by -SO3—Coated Graphene Oxide Nanosheets. ACS Sustainable Chem. Eng. 2017, 5 (8), 6597—6604.
- (52) Zhou, H. C.; Long, J. R.; Yaghi, O. M. Introduction to Metal-Organic Frameworks. *Chem. Rev.* **2012**, *112*, 673–674.
- (53) Chen, B.; Yang, Z.; Zhu, Y.; Xia, Y. Zeolitic Imidazolate Framework Materials: Recent Progress in Synthesis and Applications. *J. Mater. Chem. A* **2014**, *2*, 16811–16831.
- (54) Park, K. S.; Ni, Z.; Côté, A. P.; Choi, J. Y.; Huang, R.; Uribe-Romo, F. J.; Chae, H. K.; O'Keeffe, M.; Yaghi, O. M. Exceptional Chemical and Thermal Stability of Zeolitic Imidazolate Frameworks. *Proc. Natl. Acad. Sci. U. S. A.* **2006**, *103* (27), 10186–10191.
- (55) Bao, Q.; Lou, Y.; Xing, T.; Chen, J. Rapid Synthesis of Zeolitic Imidazolate Framework-8 (ZIF-8) in Aqueous Solution via Microwave Irradiation. *Inorg. Chem. Commun.* **2013**, *37*, 170–173.
- (56) Guo, X.; Xing, T.; Lou, Y.; Chen, J. Controlling ZIF-67 Crystals Formation through Various Cobalt Sources in Aqueous Solution. *J. Solid State Chem.* **2016**, 235, 107–112.
- (57) Zhou, K.; Mousavi, B.; Luo, Z.; Phatanasri, S.; Chaemchuen, S.; Verpoort, F. Characterization and Properties of Zn/Co Zeolitic Imidazolate Frameworks vs. ZIF-8 and ZIF-67. *J. Mater. Chem. A* **2017**, *5* (3), 952–957.
- (58) Khan, A.; Ali, M.; Ilyas, A.; Naik, P.; Vankelecom, I. F. J.; Gilani, M. A.; Bilad, M. R.; Sajjad, Z.; Khan, A. L. ZIF-67 Filled PDMS Mixed Matrix Membranes for Recovery of Ethanol via Pervaporation. *Sep. Purif. Technol.* **2018**, 206, 50–58.
- (59) Sann, E. E.; Pan, Y.; Gao, Z.; Zhan, S.; Xia, F. Highly Hydrophobic ZIF-8 Particles and Application for Oil-Water Separation. Sep. Purif. Technol. 2018, 206, 186–191.
- (60) Matatagui, D.; Sainz-Vidal, A.; Gràcia, I.; Figueras, E.; Cané, C.; Saniger, J. Improving Sensitivity of a Chemoresistive Hydrogen Sensor by Combining ZIF-8 and ZIF-67 Nanocrystals. *Proceedings* **2017**, *1* (4), 462.
- (61) Methane/Propane Double Hydrate | Janda Lab. https://ps.uci.edu/group/kcjanda/research/methanepropane-double-hydrate (accessed May 18, 2020).
- (62) Erkartal, M.; Erkilic, U.; Tam, B.; Usta, H.; Yazaydin, O.; Hupp, J. T.; Farha, O. K.; Sen, U. From 2-Methylimidazole to 1,2,3-Triazole: A Topological Transformation of ZIF-8 and ZIF-67 by Post-Synthetic Modification. *Chem. Commun.* **2017**, 53 (12), 2028–2031.
- (63) Nguyen, N. N.; Galib, M.; Nguyen, A. V. Critical Review on Gas Hydrate Formation at Solid Surfaces and in Confined Spaces Why and How Does Interfacial Regime Matter? *Energy Fuels* **2020**, 34 (6), 6751–6760.
- (64) Khay, I.; Chaplais, G.; Nouali, H.; Ortiz, G.; Marichal, C.; Patarin, J. Assessment of the Energetic Performances of Various ZIFs with SOD or RHO Topology Using High Pressure Water Intrusion-Extrusion Experiments. *Dalt. Trans.* **2016**, *45* (10), 4392–4400.
- (65) Klinowski, J.; Almeida Paz, F. A.; Silva, P.; Rocha, J. Microwave-Assisted Synthesis of Metal-Organic Frameworks. *Dalton Transactions* **2011**, *40*, 321–330.

- (66) Ni, Z.; Masel, R. I. Rapid Production of Metal-Organic Frameworks via Microwave-Assisted Solvothermal Synthesis. *J. Am. Chem. Soc.* **2006**, *128* (38), 12394–12395.
- (67) Xie, Z.; Zhu, M.; Nambo, A.; Jasinski, J. B.; Carreon, M. A. Microwave-Assisted Synthesized SAPO-56 as a Catalyst in the Conversion of CO2 to Cyclic Carbonates. *Dalt. Trans.* **2013**, 42 (19), 6732–6735.
- (68) Deshmane, C. A.; Jasinski, J. B.; Carreon, M. A. Microwave-assisted synthesis of nanocrystalline mesoporous gallium oxide. *Microporous Mesoporous Mater.* **2010**, *130* (1–3), 97–102.
- (69) Lucero, J.; Osuna, C.; Crawford, J. M.; Carreon, M. A. Microwave-Assisted Synthesis of Porous Organic Cages CC3 and CC2. CrystEngComm 2019, 21 (31), 4534–4537.
- (70) Qian, J.; Sun, F.; Qin, L. Hydrothermal Synthesis of Zeolitic Imidazolate Framework-67 (ZIF-67) Nanocrystals. *Mater. Lett.* **2012**, 82, 220–223.
- (71) Llewellyn, P.; Reinoso, F.; Rouqerol, J.; Seaton, N. Characterization of Porous Solids VII: Proceedings of the 7th International Symposium on the Characterization of Porous Solids (COPS-VII), Aix-En-Provence; Elsevier Science, 2006.
- (72) Lachance, J. Investigation of Gas Hydrates Using Differential Scanning Calorimetry with Water-in-Oil Emulsions; Colorado School of Mines: Golden, CO, 2008.
- (73) Gupta, A.; Lachance, J.; Sloan, E. D.; Koh, C. A. Measurements of Methane Hydrate Heat of Dissociation Using High Pressure Differential Scanning Calorimetry. *Chem. Eng. Sci.* **2008**, *63* (24), 5848–5853.
- (74) An, H.; Park, S.; Kwon, H. T.; Jeong, H. K.; Lee, J. S. A New Superior Competitor for Exceptional Propylene/Propane Separations: ZIF-67 Containing Mixed Matrix Membranes. *J. Membr. Sci.* **2017**, 526, 367–376.
- (75) Zhang, K.; Lively, R. P.; Zhang, C.; Koros, W. J.; Chance, R. R. Investigating the Intrinsic Ethanol/Water Separation Capability of ZIF-8: An Adsorption and Diffusion Study. *J. Phys. Chem. C* **2013**, 117 (14), 7214–7225.
- (76) Tu, M.; Wannapaiboon, S.; Khaletskaya, K.; Fischer, R. A. Engineering Zeolitic-Imidazolate Framework (ZIF) Thin Film Devices for Selective Detection of Volatile Organic Compounds. *Adv. Funct. Mater.* **2015**, 25 (28), 4470–4479.
- (77) Koh, C. A.; Wisbey, R. P.; Wu, X.; Westacott, R. E.; Soper, A. K. Water Ordering around Methane during Hydrate Formation. *J. Chem. Phys.* **2000**, *113* (15), 6390–6397.
- (78) Bai, D.; Chen, G.; Zhang, X.; Sum, A. K.; Wang, W. How Properties of Solid Surfaces Modulate the Nucleation of Gas Hydrate. *Sci. Rep.* **2015**, *5* (1), 1–12.
- (79) Liang, S.; Rozmanov, D.; Kusalik, P. G. Crystal Growth Simulations of Methane Hydrates in the Presence of Silica Surfaces. *Phys. Chem. Chem. Phys.* **2011**, *13* (44), 19856–19864.
- (80) Pérez-Pellitero, J.; Amrouche, H.; Siperstein, F. R.; Pirngruber, G.; Nieto-Draghi, C.; Chaplais, G.; Simon-Masseron, A.; Bazer-Bachi, D.; Peralta, D.; Bats, N. Adsorption of CO2, CH4, and N2 on Zeolitic Imidazolate Frameworks: Experiments and Simulations. *Chem. Eur. J.* 2010, 16 (5), 1560–1571.
- (81) Uchida, T.; Ebinuma, T.; Ishizaki, T. Dissociation Condition Measurements of Methane Hydrate in Confined Small Pores of Porous Glass. *J. Phys. Chem. B* **1999**, *103* (18), 3659–3662.
- (82) Kwon, T.-H.; Cho, G.-C.; Santamarina, J. C. Gas Hydrate Dissociation in Sediments: Pressure-Temperature Evolution. *Geochem., Geophys., Geosyst.* **2008**, 9 (3), 2007GC001920.
- (83) Park, T.; Lee, J. Y.; Kwon, T. H. Effect of Pore Size Distribution on Dissociation Temperature Depression and Phase Boundary Shift of Gas Hydrate in Various Fine-Grained Sediments. *Energy Fuels* **2018**, 32 (4), 5321–5330.
- (84) Uchida, T.; Ebinuma, T.; Takeya, S.; Nagao, J.; Narita, H. Effects of Pore Sizes on Dissociation Temperatures and Pressures of Methane, Carbon Dioxide, and Propane Hydrates in Porous Media. *J. Phys. Chem. B* **2002**, *106* (4), 820–826.
- (85) Fairen-Jimenez, D.; Moggach, S. A.; Wharmby, M. T.; Wright, P. A.; Parsons, S.; Düren, T. Opening the Gate: Framework Flexibility

- in ZIF-8 Explored by Experiments and Simulations. *J. Am. Chem. Soc.* **2011**, 133 (23), 8900–8902.
- (86) Awadallah-F, A.; Hillman, F.; Al-Muhtaseb, S. A.; Jeong, H. K. Adsorption Equilibrium and Kinetics of Nitrogen, Methane and Carbon Dioxide Gases onto ZIF-8, Cu10%/ZIF-8, and Cu30%/ZIF-8. *Ind. Eng. Chem. Res.* **2019**, *58* (16), 6653–6661.
- (87) Feng, X.; Carreon, M. A. Kinetics of Transformation on ZIF-67 Crystals. J. Cryst. Growth 2015, 418, 158–162.